HHS Public Access

Author manuscript

Neuroimage. Author manuscript; available in PMC 2016 May 01.

Published in final edited form as:

Neuroimage. 2015 May 1; 111: 476–488. doi:10.1016/j.neuroimage.2015.01.057.

Introducing Co-Activation Pattern Metrics to Quantify Spontaneous Brain Network Dynamics

Jingyuan E. Chen[a,b], **Catie Chang**[c], **Michael D. Greicius**[d], and **Gary H. Glover**[a]

[a]Department of Radiology, Stanford University, Stanford, CA 94305, USA

[b]Department of Electrical Engineering, Stanford University, Stanford, CA 94305, USA

[c]Advanced MRI Section, Laboratory of Functional and Molecular Imaging, National Institute of Neurological Disorders and Stroke, National Institutes of Health, Bethesda, MD 20892, USA

[d]Functional Imaging in Neuropsychiatric Disorders Lab, Department of Neurology and Neurological Sciences, Stanford School of Medicine, Stanford, CA 94305, USA

Abstract

Recently, fMRI researchers have begun to realize that the brain's intrinsic network patterns may undergo substantial changes during a single resting state (RS) scan. However, despite the growing interest in brain dynamics, metrics that can quantify the variability of network patterns are still quite limited. Here, we first introduce various quantification metrics based on the extension of co-activation pattern (CAP) analysis, a recently proposed point-process analysis that tracks state alternations at each individual time frame and relies on very few assumptions; then apply these proposed metrics to quantify changes of brain dynamics during a sustained 2-back working memory (WM) task compared to rest. We focus on the functional connectivity of two prominent RS networks, the default-mode network (DMN) and executive control network (ECN). We first demonstrate less variability of global Pearson correlations with respect to the two chosen networks using a sliding-window approach during WM task compared to rest; then we show that the macroscopic decrease in variations in correlations during a WM task is also well characterized by the combined effect of a reduced number of dominant CAPs, increased spatial consistency across CAPs, and increased fractional contributions of a few dominant CAPs. These CAP metrics may provide alternative and more straightforward quantitative means of characterizing brain network dynamics than time-windowed correlation analyses.

Keywords

brain dynamics; resting state networks; co-activation patterns; point process analysis; working memory

Corresponding author: Jingyuan Chen, M.S. Lucas MRI/S Center MC 5488, 1201 Welch Road Stanford, CA 94305-5488 Tel: 650 723-7577 Fax: 650 736-7925 cjy2010@stanford.edu.

1 Introduction

Intrinsic networks observed in the resting state (RS) have been intensively explored in the past two decades (for reviews, see (Biswal, 2012; van den Heuvel and Hulshoff Pol, 2010)), and have contributed enormously to the understanding of brain function. Until recently, all such studies have relied on the key assumption of temporal constancy. However, it was recently observed that RS network patterns may exhibit substantial changes across a single scan (Allen et al., 2014; Chang and Glover, 2010; Smith et al., 2012), and investigations on anesthetized animals (Hutchison et al., 2013b; Keilholz et al., 2013; Majeed et al., 2011) further demonstrated the functional relevance of such phenomena. Complementary to the conventional approaches, which integrate time series signals across the entire scan, the wealth of information carried by widely observed brain dynamics has great potential to unveil new understanding in cognitive and clinical applications (Holtzheimer and Mayberg, 2011; Rubinov and Sporns, 2011; Sakoglu et al., 2010).

Despite the growing interest in resting brain dynamics, analysis strategies and metrics to quantify the temporal variations are still quite limited. The most common approaches focus on the temporal changes of different quantification measures in a sliding sequence of truncated time windows (Chang and Glover, 2010; Handwerker et al., 2012; Hutchison et al., 2013b; Jones et al., 2012). However, sliding window methods always suffer from tradeoffs between the statistical significance achievable in a short duration window (e.g. there are approximately 10 time points in a 20s window with conventional TR sampling rate) and the reduction in high frequency content obtained as the window duration is increased (for a review, see (Hutchison et al., 2013a)). As for other multivariate approaches such as temporal independent component analysis (ICA) (Smith et al., 2012), due to the nature of model assumptions (sub-components are non-Gaussian) and lack of clear interpretations of network behavior (the correspondence between temporally independent components and the repertoire of brain states is not verified yet), it is not straightforward and requires caution to summarize the associated results for use in routine investigations of brain dynamics.

Very recently, some studies looking at resting state functional connectivity have begun to focus on those time frames when the spontaneous BOLD signal in a voxel or region exhibits relatively large amplitude. By deconvolving the task hemodynamic response function from the rest data, (Petridou et al., 2013) have identified a series of ‘spontaneous events’ and demonstrated the contribution of these events to the correlation strength and power spectra of the slow spontaneous fluctuations. Furthermore, (Tagliazucchi et al., 2012) have shown that using such spontaneous events allows one to recover those resting-state networks computed with continuous slow fluctuations across the whole scan. More elegantly, (Liu and Duyn, 2013) proposed co-activation pattern (CAP) analysis, which offers an alternative to the conventional linear correlation analysis and novel insights into the dynamic changes of the on-going network patterns. Briefly, the authors suggested that conventional linear correlation results (seed-voxel based whole brain correlation) can be computed by temporally averaging the whole brain spatial maps at a few critical time points when the seed signal intensity surpasses a certain threshold, and demonstrated that multiple stable spatial patterns (referred to as co-activation patterns, or CAPs) can be obtained by temporal

decomposition (clustering) of these critical time frames. Compared to the sliding-window approach and other multivariate approaches, e.g. temporal ICA, CAP analysis promises the examination of state alternations closer to the temporal resolution of individual time frames but relies on very few model assumptions. Furthermore, the variations of different spatial patterns and their associated fractional scan time durations (number of samples of a CAP / total number of TRs), or temporal fractions (Liu et al., 2013) provide richer quantification measures of brain dynamics that are inherently simple to interpret.

Promising as it may seem, several technical concerns potentially prevent CAPs from facilitating routine examination/quantification of brain dynamics: the enormous feature dimension (total number of gray matter voxels) in temporal clustering imposes intensive computational load and may not support data acquisitions at higher temporal/spatial resolutions; the spatial patterns and temporal fractions of the resolved CAPs are sensitive to the choice of temporal clustering numbers.

The primary focus of the current study is therefore to extend and synthesize information inherent in the CAP concepts, and provide a framework to quantify brain dynamics in routine neuroimaging investigations. To demonstrate that the proposed metrics based on CAPs can reveal more elaborate changes in brain repertoire than is shown by sliding-window correlation analysis, we apply both approaches to compare the variability of functional connectivity of two RS networks (the default-mode network (DMN) and executive control network (ECN)) at rest to that of a sustained 2-back working memory (WM) task. As the WM task enforces a control state with more engaged cognitive processing than that of rest, where uncontrolled changes in vigilance may cause significant state fluctuations (Chang et al., 2013; Wong, 2013), we anticipate that prominent differences in brain dynamics will be observed between the two mental conditions, thereby affording a means to demonstrate the value of the proposed metrics.

2 Material and Methods

2.1 Extension of CAP analysis

2.1.1 A brief introduction of CAP analysis—In conventional seed-based correlation analysis, the network patterns associated with a given seed are typically estimated by the linear correlation between the time series of each gray matter voxel and the referenced seed. The CAP method (Liu and Duyn, 2013) demonstrates that identical network patterns can be obtained by voxel-wise averaging the spatial maps of those time frames when the seed signal intensity surpasses a certain threshold (see Fig. 1A for illustration). Temporal clustering of those extracted time frames based on their spatial similarity can yield multiple spatial patterns (Fig. 1B), which are conjectured to be functionally relevant and reflect co-activation patterns (CAPs) across the whole brain at each individual time frame.

2.1.2 ROI-wise CAPs—The CAPs demonstrated by (Liu and Duyn, 2013) were obtained from maps based on correlations between a seed and every voxel. However, as shown in Fig.1, those CAPs exhibit identifiable structures that are regionally homogeneous, motivating the use of an “ROI-wise” CAPs analysis, wherein the brain is parcellated into multiple fixed ROIs, and the average signal intensity of all the voxels within each ROI

(instead of the raw signal intensity of each voxel) is taken as the feature set for K-means temporal clustering.

In contrast to the original voxel-wise CAPs, ROI-wise CAPs can provide increased spatial signal to noise ratio (SNR) in local brain regions, and more importantly, enhance the overall computational efficiency (the feature size has been reduced from # of whole gray matter voxels to # of ROIs used), which is essential for extension into larger datasets. With a surrogate dataset, we demonstrate that a whole brain ROI-wise CAP analysis provides similar results to a voxel-wise CAP analysis (section 2.2.7 CAP analysis and supplementary Fig. S1, S2).

2.1.3 Quantifiable metrics of brain dynamics in CAPs

2.1.3.1 Information in the spatial patterns of CAPs: The spatial patterns of CAPs explicitly reflect the repertoire of brain states across the whole scan. The spatial similarity between different CAPs and the quantity of CAPs that actually dominate the brain repertoire reflect the extent of network changes incurred by a switch from one state to another, and can therefore be utilized as metrics to quantify brain dynamics.

Unfortunately, in common with other data-driven approaches, e.g. ICA, the derived spatial patterns are dependent on the choice of cluster number *k* in the CAP analysis. To eliminate the bias from choosing specific *k* s, we introduce the concept of "overall dominant CAP-set", which is a set of CAPs synthesized across the results from different choices of *k* s and is representative of brain repertoires across the whole scan.

Specifically, the "overall dominant CAP-set" can be extracted in a two-stage hierarchical procedure. First, the "dominant CAP-set" associated with each cluster number *k* (see Fig. 2) is generated. Briefly, after re-ranking the CAPs by their temporal fractions (TF) in descending orders – CAP^1, CAP^2, ... CAP^k, we calculate the series of temporal frame averages $\{S_m\}_{1\le m\le k}$ as:

$$S_m=\sum_{1\le i\le m} SM_i \cdot TF_i \quad \text{Eqn. (1)}$$

where SM_i is the spatial map of CAP^i. The spatial similarity (linear Pearson correlation between the spatial patterns, i.e. the intensity patterns across all the gray matter voxels) of $\{S_m\}_{1\le m\le k}$ with the overall time frame average (S_k , i.e. the spatial map generated by averaging all the extracted time frames for CAP analysis) is further calculated as $\{s_m^s\}_{1\le m\le k}$. The dominant CAP-set of cluster number *k* is chosen as the set of CAPs $\{CAP^j\}_{1\le j\le n}$ with $\{r_{n-1}^s<rthress \& \{p \ge n\boldsymbol{I}\{rps \ge rthress\}\}$ (where *rthress* is a fixed threshold to remove miscellaneous CAPs with relatively low temporal fractions, or signal intensities that do not contribute much to the overall network pattern, and $\boldsymbol{I}$ denotes the indicator function, i.e. $\boldsymbol{I} = 1$ when $r_p^s \ge r_{rhres}^s$, 0 otherwise). At the second stage, the most reproducible pattern (the quantity of CAPs and spatial similarity) among all the dominant CAP-sets (for different *k* s) derived from the first stage is chosen as the "overall dominant CAP-set".

As a synthesized measure, the number of overall dominant CAPs reflects the diversity of network patterns (the fewer number of CAPs, the sparser the dictionary of network patterns), while the spatial consistency across different CAPs indirectly quantifies the uniformity of brain dynamics during CAP alternations (the higher spatial consistency, the less extreme dynamics that state alternations may incur).

2.1.3.2 Information in the temporal patterns of CAPs: In addition to the spatial patterns, the accompanying temporal information may also quantify the strength of brain dynamics. A first metric involves the temporal fractions (TF) of different CAPs, which quantify the number of different brain functional modes during the scan. A skewed distribution of CAP TFs, particularly with one (or a few) CAP(s) of overwhelming TF(s), may correspond to a state with more consistent network patterns (less dynamic) compared to those with more equally distributed CAP TFs. A second metric is the frequency of state alternations (FA) in CAPs. Because every abrupt switch of brain state may contribute considerable variation to the observed correlation values, a state with more frequent state alternations may likely be more dynamic compared to those with fewer alternations of states. Thus, FA can also serve as an informative metric to reveal the relative strength of brain dynamics.

Unfortunately, unlike the spatial patterns of dominant CAPs that are more consistent across different cluster number *k* s, the TFs and FAs of dominant CAPs depend significantly on the choice of specific cluster numbers. It is therefore hard to quantify the results simply, as we do for spatial patterns. A less optimum way is to employ extra criteria, e.g. silhouette score (a measure of how well a member fits in a cluster (Rousseeuw, 1987)), to select the most representative cluster number that can characterize the structure of the data, and estimate TF and FA under the specific case.

2.2 Experiments and Analysis

2.2.1 Subjects—Twenty one healthy subjects (10 females, aged 31±10 years) recruited from the Stanford community participated in the current study. All subjects provided written, informed consent, using a protocol approved by the Stanford Institutional Review Board.

2.2.2 Imaging parameters—FMRI data were collected at a 3T scanner with an 8-channel radio frequency coil (GE Discovery 750, Milwaukee, WI). Thirty-one oblique axial slices were acquired with 4-mm slice thickness, 1mm-skip. T2-weighted fast spin echo structural images (TR = 3000 ms, TE = 68 ms, ETL = 12, FOV = 22cm, matrix 192×256) were acquired for anatomical reference. A gradient echo spiral-in/out pulse sequence (Glover and Law, 2001) was used for T2*-weighted functional imaging (TR = 2000 ms, TE = 30 ms, flip angle = 77°, matrix 64×64, FOV = 22 cm, same slice prescription as the anatomical image). Subjects' motions were minimized with a bite bar (the average of root mean square translations were less than 70 microns across all scans). Respiration and cardiac (pulse oximetry) data were recorded using the scanner's built-in physiological monitoring system.

2.2.3 Task paradigm—All subjects underwent (1) an 8-min rest scan, for which they were instructed to remain awake, devoid of systematic thinking, and keep eyes closed; (2) a

2-back working memory (WM) task scan, during which they were instructed to judge whether a currently-present letter was identical to the one presented two letters back during the task condition (see supplementary Fig. S3). The WM task scan has two parts: the first of which is a block design (to target brain regions activated during WM tasks, block duration 48s, 7 blocks); the second part is an 8-min continuous WM task (inter-stimulus interval (ISI) = 3s, for comparison with rest data). The block design and continuous task were separated by a 30s rest period (see supplementary Fig. S3 for detailed scheme). To prevent interference from the prior cognitive load on the ensuing resting-state spontaneous activity, the task scans were performed after rest scans for all the subjects.

2.2.4 Preprocessing—Datasets from both rest and WM task scans were preprocessed using custom C and Matlab routines. The first 10 frames of each scan were discarded to allow the MR signal to achieve T1 equilibration. Standard preprocessing included slice-time correction, physiological noise correction with both RETROICOR (Glover et al., 2000) and RVHRCOR (Chang et al., 2009), and nuisance regression of scan drifts (linear and quadratic trends), six head motion parameters, signals extracted from white matter and CSF (3-mm radius spheres centered at MNI (26, -12, 35) and (19, -33, 18), renormalized to each subject's native space using SPM5 (Wellcome Department of Cognitive Neurology, London)). Subjects' behavioral time series (reaction time sequence convolved with the hemodynamic response function) (Chen et al., 2013) were also regressed out of the WM task data. Datasets were further spatially smoothed using a 3D Gaussian kernel (FWHM = 4mm). Both the rest and WM task datasets were low-pass filtered to remove frequencies above 0.1 Hz.

2.2.5 Defining network regions of interest

2.2.5.1 Default-mode network: A 6mm-radius sphere (MNI (-6, -58, 28)) in the posterior cingulate cortex (PCC) was selected as the primary ROI for the DMN. The coordinate was first reported by a meta-analysis study of task-based co-activation with DMN regions (Toro et al., 2008), and verified in our datasets to produce robust positive correlations within DMN and negative correlations between DMN and task-positive networks (see Fig. 3A).

2.2.5.2 Executive-control network: A 6mm-radius sphere (MNI (34, -54, 46)) in the right angular gyrus was adopted as the primary ROI for the ECN. The center coordinate was a local maxima in the group-level activation map from the random-effects analysis of the block-stimulus part of the WM task (see Fig. 3B).

2.2.6 Sliding-window correlation analysis—The sliding-window correlations estimate the time-varying linear correlation between two time series (*x* and *y*) in a sequence of truncated temporal windows:

$$r^t(t) = corr\left(x_t^{t+w-1}, y_t^{t+w-1}\right) \quad \text{Eqn. (2)}$$

where *w* is the window size, x_t^{t+w-1} and y_t^{t+w-1} denote the portion of the time series from time *t* to *t+w-1*, and *corr()* denotes computation of the linear Pearson correlation coefficient (Chang and Glover, 2010). This approach was carried out with window durations of 1-min

and 2-min, and step size 4-s. Standard deviations of the windowed correlation sequences with respect to DMN/ECN seeds (see 2.2.5 defining network regions of interest) were compared across states to evaluate the macroscopic changes of brain dynamics in these two networks.

2.2.7 CAP analysis—Datasets from all 21 subjects were normalized to the MNI template and transformed to z-score (the time series of each voxel was demeaned and normalized by its temporal standard deviation). Time frames with network seed signal intensity amongst the top 31% (72 time frames) of each subject were selected and temporally concatenated to make a rest scan set and a WM task scan set for ROI-wise CAP analysis.

Two functional ROI sets with disparate extents of cortex coverage were heuristically selected for comparisons: (1) 'ROI_{90}', 90 RS network ROIs reported in (Shirer et al., 2012); (2) 'ROI_{499}', 499 ROIs with whole grey matter coverage (see supplementary Material S1 for the description of 499 ROIs, and Fig. S1 for the ROI atlas). For the rest of the paper, results derived from 90/499w ROIs are prefixed with '$ROI_{90/499w}$'. 'w' here indicates that the signal intensity within each ROI is weighted by the ROI size so that the results associated with 'ROI_{499w}' can serve as a good approximation to those generated with voxel-wise CAP analysis (see Appendix distance measures of '$ROI_{90/499w}$' in K-means clustering and supplementary Fig. S2 for demonstration).

To extract the overall dominant CAPs, we varied the number of clusters in K-means clustering from 2 to 16, and set $r^s_{thres}=0.95$ (see above 2.1.3.1 Information in the spatial patterns of CAPs). To account for the instability of single trial clustering result, for each cluster number *k*, we repeated K-means clustering 1000 times, then synthesized the 1000 classification results into one via the Normalized-cut method (http://www.cis.upenn.edu/~jshi/software/), in which the weighting between two time frames *i* and *j* is defined as:

$$w_{ij}=\sum_{\mathrm{n}=1}^{1000}\mathrm{I}_{\mathrm{n}}\left(i,j\in \text{same cluster}\right) \quad \text{Eqn. (3)}$$

where **I** is the indicator function (i.e. I = 1 when {*i*,*j* ∈ same cluster}, I = 0 otherwise), n is the nth trial of the K-means clustering. "Overall dominant CAP-set" was extracted from the results with clustering number *k* varying from 2 to 16, $r^s_{thres}=0.95$ (see above 2.1.3.1 Information in the spatial patterns of CAPs).

To choose the most representative cluster number, i.e. the number *k* that can best reflect the intrinsic structure of the datasets, we used silhouette score (see supplementary material M2) to evaluate the partition results for comparison of TF and FA in CAPs across states (Rousseeuw, 1987).

The inclusion of two functional ROI sets with disparate extents of cortex coverage was intended to alleviate the potential concern in temporal clustering: if the percentage of 'informative' metrics that help differentiate different CAPs are overwhelmed by 'noisy' metrics that are common across CAPs and contribute none to the classification, the reliability of the clustering results would be significantly degraded. This may be the case for voxel-wise CAPs because of the large number of voxels. As revealed in Liu's study, CAPs

associated with specific seeds (PCC and intraparietal sulcus) had significant overlap in wide ranges of cortical areas, implying that regions pivotal in differentiating different CAPs might only account for a relatively small fraction of the features entered into the K-means clustering, and that the inclusion of additional voxels may not add new information that can disambiguate CAPs. As will be seen later in the results section, different ROI sets did reach at inconsistent clustering results (see 3.2 WM task vs. rest: perspectives from CAPs), even different implications about changes in brain dynamics (see 3.2.2 Temporal fractions of the 1st dominant CAP).

The upper bound of examined cluster number *k* was set to be 16, based on the hypothesis that the dimension of dominant CAPs with respect to the chosen networks should be far smaller than the whole set of spontaneous states the brain may exhibit (in a prior study decomposing spontaneous CAPs of the whole brain volumes (Liu et al., 2013), cluster number *k = 30* was considered as a good choice for whole brain CAPs (the complete set of brain spontaneous activation patterns, in contrast to those associated with a specific cortical region/network, e.g. DMN/ECN-CAPs here)). Similarly, in another temporal ICA study, (Smith et al., 2012) identified 21 whole brain temporal functional modes at rest. Therefore, in our study 16 was adequate to include the dimension of dominant CAPs associated with a specific network, which includes significantly fewer voxels and time frames than the whole brain analyses discussed above.

The threshold of spatial similarity r^s_{thres} to extract dominant CAP-sets was heuristically set to be 0.95, a value high enough to demonstrate identical spatial pattern of the overall frame average (95 percentile of the distributions of between-CAP similarities were only ~0.25). To explore whether 0.95 was a reasonable r^s_{thres} in current datasets, two post-hoc analyses were performed after resolving the "overall dominant CAP-sets": (1) we also counted the number of dominant CAP-sets (for *k* varying from 2 to 16) that contained the "overall dominant CAP-sets" (selected with 0.95) as the leading subsets; (2) we ranked individual CAPs by their reproducibility across different choices of *k* s, and checked whether those within the "overall dominant CAP-sets" themselves were among the most reproducible patterns.

The threshold for choosing the time frames extracted for analysis should be considered carefully, as the time frames included for temporal clustering are impacted. In (Liu and Duyn, 2013), the authors found that using as few as the top 15% of frames replicated the average linear correlation pattern well. However, because we focused on the dynamic variability instead of the static correlation pattern here, we set a lower threshold (31%, 72 frames per scan) to establish a better correspondence to the sliding window approach, which integrates signals across the full intensity range and all time frames. To explore how sensitive current results were to the intensity threshold, DMN-CAPs with ROI_{90} were also tested with threshold 21% (48 frames per scan) and 42% (96 frames per scan).

3 Results

3.1 Variability of sliding-window correlations with respect to DMN and ECN

Fig. 4A shows the variability (standard deviations) over the sequence of 1-min sliding-window correlations between each brain voxel and the two network seeds, averaged across

21 subjects. As revealed by the group mean map, a wide range of cortical areas exhibited reduced correlation variability during sustained WM task compared to rest; however in most of these regions the differences failed to reach statistical significance in a voxel-wise Wilcoxon sign-rank test with$\alpha = 0.05$. To allow for inconsistent patterns of reduced correlation variability across the examined subjects, further analysis was carried out by counting the percentage of gray matter voxels that showed larger standard deviations during (rest > WM task) directly, and compared it against the count for (WM task > rest). Here, only voxels with absolute difference in standard deviations of the sliding-window correlation sequence |rest – WM task| surpassing a threshold of 0.1 were included. For both networks, most subjects showed overwhelming percentages of cortical regions with higher correlation variations during rest (Fig. 4B). The results remained significant ($p < 0.05$, paired t test) when the threshold of the absolute difference was varied from 0 to 0.3 for the DMN case, and 0 to 0.25 for the ECN case. The results of 2-min sliding-window were quantitatively similar – the rest state exhibited higher correlation variations with overwhelming percentages of cortical regions (see supplementary Fig. S4).

Identical sliding-window correlation analyses were also performed on the WM task datasets without projecting out the behavioral data (see 2.2.4 Preprocessing), global reduction of correlation variability as shown in Fig. 4A still persisted, suggesting that the reduced correlation variability in WM task datasets is not attributable to the extra regression of behavioral data.

3.2 WM task vs. rest: perspectives from CAPs

3.2.1 Dominant REST-CAP-sets and WM-CAP-sets—Fig. 5 shows the “overall dominant CAP-sets” associated with the DMN. Dominant CAP-sets derived from ROI_{90} and ROI_{499w} contained consistent sub-CAPs (see Table 1, $REST_{90}$ vs. $REST_{499w}$, WM_{90} vs. WM_{499w}). However, as the features for the temporal clustering were not identical, we observed subtle differences in the spatial profiles between $REST_{90}$ and $REST_{499}$, including dorsal lateral prefrontal cortex, parahippocampus gyrus, and superior parietal lobe, indicated with white arrows. WM_{90}-CAP 1 was probably split into two separate clusters (WM_{499w}-CAP 2 and WM_{499w}-CAP 4) using ROI_{499w}. In the between-scan comparison, the number of overall dominant CAPs reduced from 4 (rest) to 3 (WM task) in the ROI_{90} case, and the change was replaced by increased spatial similarity across WM-CAPs compared to rest in the ROI_{499} case.

Surprisingly, we were also able to see good correspondence between dominant REST-CAP-sets and WM-CAP-sets (see Table 1, $REST_{90}$ vs. WM_{90}, $REST_{499w}$ vs. WM_{499w}). Closer examination revealed that these pairs did not share identical spatial patterns, but had subtle differences in particular areas, including angular gyrus, precentral gyrus, inferior parietal lobe, i.e. in brain regions actively involved in the working memory task, indicated with yellow arrows.

Fig. 6 shows the “overall dominant CAP-sets” associated with the ECN. In common with the case of DMN, CAP-sets generated with ROI_{90} and ROI_{499w} contained common sub-CAPs (see Table 2, $REST_{90}$ vs. $REST_{499w}$, WM_{90} vs. WM_{499w}). Again, these patterns were

not entirely identical ($REST_{90}$-CAP 3/5 did not have matched equivalents in $REST_{499w}$-CAPs, and WM_{90}-CAP 2 was probably a mixed cluster from subsets in WM_{499w}-CAP 1/3).

Likewise, certain CAPs appeared in both scans (see Table 2, $REST_{90}$ vs. WM_{90}, $REST_{499w}$ vs. WM_{499w}), with minor deformation in the anterior part of the middle cingulate gyrus, precentral gyrus, lingual gyrus, indicated with yellow arrows in Figs. 5 and 6.

All the spatial similarities across different CAP-sets discussed above were quantitatively reflected in the covariance matrixes (Fig. 5A/B, Fig. 6A/B).

The "overall dominant CAP-sets" were generally associated with cluster number *k* ranging from 5 to 11 in most cases (see Table 3), further confirming that the selected range of *k* s (from 2 to 16) is reasonable in this study.

We did note that slight tuning of the heuristically selected threshold $r^s_{thres}=0.95$ in the extraction of "overall dominant CAP-set" may change the quantity of the extracted dominant CAPs at certain cluster numbers. Results of the post-hoc analyses (see section 2.2.7 CAP analysis) alleviated concerns that threshold choice was critical: (1) the number of dominant CAP-sets that contained the "overall dominant CAP-sets" (selected with *0.95*) as the leading subsets were listed in Table 3 (numbers in parenthesis), the selected patterns still dominated; (2) those CAPs contained in the "overall dominant CAP-sets" themselves were still among the most repeatable spatial patterns (not shown). Hence, *0.95* appears to be a reasonable choice in our dataset.

In the results of DMN-CAPs derived from ROI_{90}, sub-patterns of the "overall dominant CAP-sets" (31%) were observable for the majority of *k* s at threshold 21%/42%. Moreover, the dominant CAP-set itself as an entirety also persisted in certain *k* s (see supplementary Table S1), and dominant CAPs associated with other *k* s did not resemble the dominant CAP-set (31%): they generally varied in ways of either (one cluster split into two clusters with high spatial similarity) or (index reallocation within clusters), thus posing no violation to the conclusions drawn from threshold 31% (as will be discussed later in 4.2.1 Information in the "overall dominant CAP-sets"). Furthermore, 31% gave the most consistent dominant CAPs across different cluster numbers, as reflected in supplementary Table S1 for our datasets. These observations, together with the comparison of ROI_{90} and ROI_{499w} suggest that the CAPs may possess a very skewed distribution, with a portion of subsets much closer in similarity to one another than the others, which makes it hard to find a clear division between different clusters (Liu et al., 2013).

3.2.2 Temporal fractions of the 1st dominant CAP—As shown in Fig. 7, for both states (rest and WM task) and both networks (DMN and ECN), *k* = 2 gave the highest clustering score, which is consistent with the observations reported by (Liu and Duyn, 2013) that the REST-CAPs can generally be divided into two main categories based on their spatial resemblance.

Given the results in Fig. 7, further comparisons of temporal fractions therefore concentrated on the case when *k* = 2. The CAP with temporal fraction (TF) larger than 50% was defined as the 1st dominant CAP, and the other was defined as the 2nd dominant CAP. The spatial

patterns of CAPs derived using ROI_{90} and ROI_{499w} were remarkably consistent (spatial similarity higher than 0.95 for both networks and both $1^{st}/2^{nd}$ CAPs), while the corresponding temporal fractions were significantly ROI-dependent: The ROI_{90} yielded significantly higher TF of the 1^{st} dominant CAP during sustained WM task compared to rest for both networks (DMN $p = 0.013$, ECN $p = 3.5\times10^{-5}$); the ROI_{499w} yielded no statistically significant differences in TF for either network (DMN $p = 0.763$, ECN $p = 0.074$) in paired t-test,$\alpha = 0.05$ (see Table 4, Fig. 8A).

Given the distinct results regarding statistical significance described above, a post-hoc examination was performed to assess the potential effects that the number of ROIs (or involved cortical areas) utilized might exert on the resulting statistical significance. We first ranked all the 499 ROIs by their importance as features to differentiate the 1^{st} and 2^{nd} dominant CAPs as follows: (1) we derived subject-specific 1^{st} dominant CAPs by projecting the ROI_{499w} clustering indexes back to each subject's native temporal regime and averaging frames assigned to the 1^{st} dominant CAPs; (2) we then used a group-level paired-t test to compare differences between the spatial patterns of the 1^{st} and 2^{nd} dominant CAPs (as shown in Fig. 7B, corresponding dominant CAPs in both states exhibited very high spatial similarity, the spatial patterns of both states were hence combined and entered into a single paired-t test), and further ranked the 499 ROIs by the absolute t-values averaged within each ROI atlas. Although the subject-specific CAPs and the t-value of each ROI was generated from atlas ROI_{499w}, we argue that using clustering index derived with atlas ROI_{90} would yield no significant difference since the spatial patterns of the $1^{st}/2^{nd}$ CAPs were nearly identical for ROI_{90} and ROI_{499w} cases.

Fig. 8B shows the statistical significance (p values) for paired t-tests (temporal fractions of the 1^{st} dominant CAP during rest against WM task) as a function of ROI numbers (in descending order of absolute t values) involved in the K-means classifications. At the beginning stage, p value decreased as more and more 'informative' (high |t|-value) ROIs were employed as features for clustering, while at the later stage, p values started to increase as more 'noisy' (low |t|-value) ROIs were included and obscured the classifications. Because the ROIs are ranked in descending order of absolute t-value, i.e. descending importance as the features to differentiate the 1^{st} and 2^{nd} dominant CAPs, we therefore argue that the p values which are below 0.05 at the beginning stage are most trustworthy, and indicate significantly higher temporal fractions of the 1^{st} dominant CAPs (more consistent brain states) during WM task compared to rest in both networks.

3.2.3 Alternation frequencies of CAPs—A group-level paired t-test was performed to test whether the frequency of alternation of the CAPs (the frequency at which the brain state shifted from the current CAP to a different CAP) was significantly lower during WM task than rest and contributed to the overall reduction of correlation variations. However, no results reached statistical significance in a paired-t test with$\alpha = 0.05$ for both networks, see Table 4. Supplementary Fig. S5 shows examples of a few subjects for $k = 2$, in which the alternation frequency appears to be independent from the distribution of temporal fractions associated with different CAPs.

4 Discussion

4.1 General findings

In the present study, we introduced various metrics to quantify brain dynamics based on the extension of CAP analysis, and demonstrated the values of the proposed metrics by characterizing the changes of DMN and ECN patterns during a WM task compared to rest. Complementary to the conventional sliding-window correlation approach, which revealed more consistent network patterns in a macroscopic manner through decreased variability of linear correlations (see Fig. 4), the proposed metrics can shed additional light on the changes in the brain repertoire, including reduced number of dominant CAPs, increased spatial consistency across CAPs, and increased fractional contributions from a few dominant CAPs during WM task compared with rest.

4.2 Quantifiable metrics of brain dynamics in CAPs

Through examination of distinct spatial patterns that each time frame was assigned to, we are able to track the state alternations at each individual time frame. These variations of different CAPs and their associated temporal fractions can accommodate richer quantification measures of brain dynamics and therefore provide diversified metrics describing changes in the brain repertoire.

4.2.1 Information in the "overall dominant CAP-sets"—The concept of "overall dominant CAP-set" helps mitigate the sensitivity of results on specific cluster numbers in K-means clustering, and make CAPs robustly able to quantify brain dynamics. Specifically, the quantity of overall dominant CAPs reflects the diversity of network patterns (the fewer number of CAPs, the sparser the dictionary of network patterns) and the spatial consistency across different CAPs indirectly reveals the dynamics incurred by state alternations (the higher spatial consistency, the less extreme dynamics that state alternations may incur). Although the two aspects of information carried by the dominant CAPs (number of dominant CAPs and their spatial similarity) relate to different interpretations of brain network behavior, they are not distinguishable from the methodological perspective: in the K-means implementation, one single cluster can split into two clusters with neighboring centroids due to noise. In this case, the extracted network patterns within a CAP would not necessarily have perfect similarity with each other. If the neural origin of CAPs is indeed large-scale neuronal avalanching activity as proposed in (Liu and Duyn, 2013; Tagliazucchi et al., 2012), CAPs associated with a specific ROI may be contaminated by propagated fluctuations initiated at other brain regions.

At present, a useful view towards CAP analysis would be – it offers additional dimensions to characterize the key dynamic structures inherent in the network patterns, given that the spatial patterns of different time frames vary in a continuous manner. Table 5 summarizes the changes of "overall dominant CAP-sets" during WM task compared to rest. In line with the discussion above, the pattern of changes fell arbitrarily into either 'reduced number of dominant CAPs' or 'increased spatial consistency across different CAPs'. Both interpretations demonstrate more parsimonious brain states, i.e. more consistent network patterns, during sustained WM task compared to rest.

Apart from contributing new perspectives to quantify the extent of brain dynamics, the spatial patterns of the dominant CAP-set also offer more intuitive views (in contrast to bewildering results associated with different choices of cluster numbers) towards the changes of brain repertoire across states. In the present datasets, we surprisingly observed that certain REST-CAPs and WM-CAPs exhibited substantial spatial similarity (see Fig. 5/6 for dominant CAP-sets, Fig. 7 for CAPs under $k = 2$), and that subtle differences between these CAPs resided in brain regions typically active in a WM task. Some of the consistent CAPs across states may be induced by the bite bar or other aspects of the scan environment that cause mental discomfort or even incite head motion, although very little head motion was observed in the datasets. They may also come from other types of motion, e.g. finger movements, which can induce actual neural activation. However, the observed consistency of CAPs can not be explained by motion alone, as similar findings have been reported in recent animal studies (Liang et al., 2014; Liu et al., 2014), where certain CAPs are consistent across awake and anesthetized states in both rats and macaques. Therefore, we hypothesize that there may be a limited number of CAPs that can be considered universal across different tasks, rest states and subjects and even animals, so that, like the DMN itself, deformations of these CAPs may be relevant as biomarkers.

4.2.2 Temporal fractions (TF) of CAPs—The temporal fractions of different CAPs can be used to quantify the number of different brain states during the scan. During rest, the occurrence rates associated with different CAPs were nearly equally distributed. By contrast, during a sustained WM task, the assumed primary focus of subjects' attention was to react to the on-going WM task-trials, and it was natural to expect that the CAP tightly related to the task modulation was the most repeated spatial pattern and dominated the brain repertoire, which further led to macroscopic observations of reduced brain dynamics as well. Indeed, we were able to demonstrate significantly higher temporal fractions of the 1st dominant CAP during WM task compared to that for rest, which also exhibited increased spatial similarity with the WM task activation pattern (see Fig. 3B) – the spatial similarity r^s increased from 0.53 during WM task to 0.62 (negative correlation) at rest in the DMN case, and from 0.13 to 0.51 in the ECN case.

Here, we only reported the comparison of temporal fractions associated with the clustering number selected by silhouette scores. For certain choices of k other than silhouette score, similar comparisons result (Chen et al., 2014), although the validity of applying identical clustering numbers across states is still under debate. However, in the particular application of temporal fractions in quantifying brain dynamics, the spatial similarity between CAPs should always be considered as well, particularly in cases where certain resolved CAPs exhibit very similar structure patterns, i.e., a state switch between these CAPs may contribute a negligible increase in brain dynamics. Indeed, CAPs with similar spatial maps always engender a higher chance of misclassification. Therefore, using silhouette score, or other clustering criteria, to choose the number of clusters may better demonstrate the spatial similarity between CAPs by maximizing the relative ratio of inter- and intra-cluster distance.

4.2.3 Frequency of state alternations (FA) in CAPs—An abrupt switch of brain state may contribute considerable variations to the observed correlation values, so the frequency

of state alternations in CAPs can be taken as another informative metric to quantify the strength of brain dynamics. Although in our datasets we failed to see significantly reduced frequency of alternations during sustained WM task compared to rest despite trends towards reduced FA, this is not yet conclusive as such analysis demands strict precision of CAP allocation at every time frame, which may be compromised by SNR in a time frame and uncertainty relating to CAP estimation. For instance, in the result of subject 8 with cluster number $k = 2$ at rest (see supplementary Fig. S5), we note that one frame of interest was classified as the 1st dominant CAP (green color, indicated with red arrows) although its neighboring frames were identified as the 2nd dominant CAP (blue color), and this one instance contributed an additional two alternations to the count. Closer examination of the spatial pattern was unable to differentiate whether it was a misclassification or an accurate reflection of the on-going cognitive state. In future analyses, the precision may be improved via integration of the preceding few CAP allocations, or invoking versatile regularization constraints that can enforce reasonable state alternations based on empirical data. We also anticipate that the SNR per frame would be proportionally improved in higher field strength, e.g. 7T, and that with the growth of explorations into CAPs, deeper understanding of CAPs could guide more accurate classification of different CAPs, e.g. employing dual regression with a set of well characterized CAP templates. As discussed above, however, the timing of state alternations has great potential to characterize brain dynamics beyond alternation frequency, e.g. transition patterns across different CAPs, and may facilitate in-depth understanding towards the ordered rhythms of intrinsic spontaneous activity.

4.2.4 Interdependence of CAP metrics—Although the new metrics introduced in this study – the quantity of and spatial similarity within the overall dominant CAP-set, the distribution of temporal fractions, and the frequency of alternations in CAPs – each provide a new dimension to quantify brain dynamics, they are not independent by nature. As discussed above (4.2.1 Information in the “overall dominant CAP-sets”), the spatial patterns of the extracted time frames for CAP analysis vary in a continuous manner, but CAPs “aggressively” attempt to cluster these time frames into discrete sets, so the quantity of overall dominant CAPs and the spatial consistency across CAPs are not strictly separable. If two CAPs contained in the overall dominant set have very high spatial similarity, they may likely be classified in the same CAP under k selected by the silhouette score and contribute to a skewed distribution of TFs. In this regard, spatial similarity within the “overall dominant CAP-set” shares common information with the distribution of TFs.

We also note that these metrics taken separately may not fully describe brain dynamics, although in the rest vs. WM task case, all the metrics suggest more consistent network patterns (reduced dynamics) during the WM task. Imagine an extreme and simple comparison of two scans: scan A consisting of a “task 1” block followed by a “task 2” block, while scan B consists of “task 1” and “task 2” trials alternating in an interleaved fashion. Ideally, these two scans will result in two dominant CAPs corresponding to “task 1” and “task 2” respectively, and scan A will have a similar number of TFs as scan B but a less intensive FA in CAPs. Therefore, the distribution of TFs infers no difference of brain dynamics for the two scans while FA in CAPs reflects less dynamic network patterns in scan A compared to B.

From the foregoing discussion, it may appear difficult to quantify the relative importance of the different metrics. Fundamentally, the study of brain dynamics is still at quite an exploratory stage, with very little known about its projection onto the proposed quantification dimensions. However, such uncertainty again demonstrates the necessity of more elaborate perspectives in studying brain dynamics. Given the limited knowledge about brain dynamics at present, we suggest all the proposed metrics be combined to offer a more comprehensive view towards the changes of brain repertoire.

4.3 Voxel-wise vs. ROI-wise CAPs

In lieu of deriving CAPs based on thousands of individual voxels from the entire brain, we showed that an ROI-based analysis provided similar results. Apart from increasing the spatial SNR in local areas, another evident advantage of ROI-wise CAP analysis is that it greatly reduces the computational load involved in the clustering analysis, thus making analyses of larger datasets feasible, e.g. with higher temporal sampling rates. The rationale behind ROI-wise CAP analysis is based on the key assumption that the employed ROI atlas is able to capture intrinsic functional structures pertaining to the object of interest, i.e., regions pivotal in differentiating distinct CAPs are identifiable and occupy complete units in the proposed atlas; otherwise, averaged information across heterogeneous sub-regions within an ROI may result in reduced predictability/statistical power instead. Because ROI_{90} and ROI_{499} utilized here employed a limited number of vigilance states for their delineation (4 subjectively-driven cognitive states, see (Shirer et al., 2012) for detailed descriptions), their validity as atlases for CAP analysis warrants examinations in broader mental states.

Another implication of the present findings is that metrics associated with CAPs (more fundamentally the clustering results) may vary as a function of cortical areas encompassed in the features of temporal clustering. Both results presented here and in (Liu and Duyn, 2013) suggest that certain CAPs overlap in a wide range of grey matter regions, and further raise the concern that in cases where the vast majority of features are pure ‘noise’ (common neural information shared by different spatial patterns), the performance of temporal clustering may be degraded and yield spurious conclusions. The problem turns out to be more prominent in the temporal fractions (Fig. 8) compared to the spatial patterns of resolved CAPs (Fig. 5, 6, 7B), which may be explained by the fact that in the calculation of temporal fractions, well classified and misclassified temporal frames are taken equally; while in deriving the spatial patterns (frame average within the same cluster), well classified temporal frames typically exhibit higher contrast compared to misclassified temporal frames in cortical regions pivotal in distinguishing between different CAPs, which naturally suppress the influence from misclassified frames.

Collectively, further efforts will be required to focus on developing a case-specific CAP analysis scheme, which is potentially challenging without any prior knowledge of the question being addressed. Promising solutions might invoke concepts from hierarchical clustering, or combining ROI-wise and voxel-wise CAP analysis in a hybrid manner. Importantly, given that we cannot predict ahead of time whether one cortical region is ‘informative’ or ‘noisy’ in clustering, a post-hoc examination of the CAP results as

performed herein (see results, temporal fraction of the 1st dominant CAP above) is highly recommended.

5 Conclusion

In the present study, we introduced four metrics to quantify brain dynamics based on CAP analysis, which can offer more elaborate descriptions of brain network dynamics than simple sliding-window correlation coefficients. Although here we focused on the functional connectivity with respect to two specific networks under sustained WM task and rest, the proposed framework of analysis and quantitative metrics of brain dynamics may be generalized to other brain networks and mental states.

Supplementary Material

Refer to Web version on PubMed Central for supplementary material.

Acknowledgments

The authors gratefully acknowledge Bernard Ng and William Shirer for providing the brain functional atlas (ROI499w), the NIH for funding support (P41 EB015891), and three anonymous reviewers for their constructive comments, which have substantially improved the quality of the manuscript.

Appendix

Distance measures of '$ROI_{90/499w}$' in K-means clustering

ROI_{90}

Let $\boldsymbol{I^x_{90}} = (i^x_1, i^x_2, \ldots, i^x_{90})$ and $\boldsymbol{I^y_{90}} = (i^y_1, i^y_2, \ldots, i^y_{90})$ denote the vectors of signal intensities averaged within each of 90 functional ROIs (ROI_{90}) at temporal frame *x* and *y* respectively. Then the distance measure $d^{90}_{x.y}$ between two temporal frames *x* and *y* in K-means temporal clustering is defined as 1 minus the linear Pearson correlation coefficient between vector $\boldsymbol{I^x_{90}}$ and $\boldsymbol{I^y_{90}}$.

ROI_{499w}

Similarly, let $\boldsymbol{I^x_{499}} = (i^x_1, i^x_2, \ldots, i^x_{499})$ and $\boldsymbol{I^y_{499}} = (i^y_1, i^y_2, \ldots, i^y_{499})$ denote the vectors of signal intensities averaged within each of 499 functional ROIs (ROI_{499}) at temporal frame *x* and *y* respectively, and let $\boldsymbol{V} = (v_1, v_2, \ldots, v_{499})$ denote the voxel volume of each ROI. We then generate two new sets of vectors:

$$\boldsymbol{I^x_{499w}} = (i^x_{1w}, i^x_{2w}, \ldots, i^x_{499w}) \quad \text{and} \quad \boldsymbol{I^y_{499w}} = (i^y_{1w}, i^y_{2w}, \ldots, i^y_{499w}),$$
$$\text{with} \quad i^x_{kw} = \left(i^x_k - \overline{\boldsymbol{I^x}}\right) \cdot \sqrt{v_k}, i^y_{kw} = \left(i^y_k - \overline{\boldsymbol{I^y}}\right) \cdot \sqrt{v_k}, \quad \text{for} \quad 1 \le k \le 499$$
$$\text{where} \quad \overline{\boldsymbol{I^x}} = \frac{\sum_{k=1}^{499} I^x_k \cdot v_k}{\sum_{k=1}^{499} v_k} \quad \text{and} \quad \overline{\boldsymbol{I^y}} = \frac{\sum_{k=1}^{499} i^y_k \cdot v_k}{\sum_{k=1}^{499} v_k}.$$

The distance measure $d^{499w}_{x,y}$ between two temporal frames *x* and *y* in K-means clustering is defined as:

$$d_{x,y}^{499w}=1-\frac{\sum_{k=1}^{499} i_{kw}^{x}\cdot i_{kw}^{y}}{\sqrt{\left(\sum_{k=1}^{499}\left(i_{kw}^{x}\right)^{2}\right)\cdot\left(\sum_{k=1}^{499}\left(i_{kw}^{y}\right)^{2}\right)}}=1-\frac{\boldsymbol{I}_{499w}^{x}\cdot\boldsymbol{I}_{499w}^{y\prime}}{\sqrt{\left(\boldsymbol{I}_{499w}^{x}\cdot\boldsymbol{I}_{499w}^{x\prime}\right)\cdot\left(\boldsymbol{I}_{499w}^{y}\cdot\boldsymbol{I}_{499w}^{y\prime}\right)}}$$

Through a few simple transformations, one can demonstrate that $1-d_{x,y}^{499w}$ approximates the voxel-wise linear Pearson correlation (each gray matter voxel is taken as an individual feature/element) between temporal frame *x* and *y*, except that each voxel's intensity is now replaced by the mean value of the corresponding functional ROI.

References

Allen EA, Damaraju E, Plis SM, Erhardt EB, Eichele T, Calhoun VD. Tracking whole-brain connectivity dynamics in the resting state. Cereb Cortex. 2014; 24:663–676. [PubMed: 23146964]

Biswal BB. Resting state fMRI: a personal history. Neuroimage. 2012; 62:938–944. [PubMed: 22326802]

Chang C, Cunningham JP, Glover GH. Influence of heart rate on the BOLD signal: the cardiac response function. Neuroimage. 2009; 44:857–869. [PubMed: 18951982]

Chang C, Glover GH. Time-frequency dynamics of resting-state brain connectivity measured with fMRI. Neuroimage. 2010; 50:81–98. [PubMed: 20006716]

Chang C, Liu Z, Chen MC, Liu X, Duyn JH. EEG correlates of time-varying BOLD functional connectivity. Neuroimage. 2013; 72:227–236. [PubMed: 23376790]

Chang C, Thomason ME, Glover GH. Mapping and correction of vascular hemodynamic latency in the BOLD signal. Neuroimage. 2008; 43:90–102. [PubMed: 18656545]

Chen, J.; Chang, C.; Glover, GH. Spontaneous Low-frequency Functional Connectivity and Temporal Dynamics: Working Memory vs. Rest. International Society for Magnetic Resonance in Medicine; United States: Apr. 2013

Chen, J.; Glover, GH. Weaker Brain Dynamics during Sustained Working Memory Task: Perspectives from Co-activation Patterns. International Society for Magnetic Resonance in Medicine; Italy: May. 2014

Glover GH, Law CS. Spiral-in/out BOLD fMRI for increased SNR and reduced susceptibility artifacts. Magn Reson Med. 2001; 46:515–522. [PubMed: 11550244]

Glover GH, Li TQ, Ress D. Image-based method for retrospective correction of physiological motion effects in fMRI: RETROICOR. Magn Reson Med. 2000; 44:162–167. [PubMed: 10893535]

Handwerker DA, Roopchansingh V, Gonzalez-Castillo J, Bandettini PA. Periodic changes in fMRI connectivity. Neuroimage. 2012; 63:1712–1719. [PubMed: 22796990]

Holtzheimer PE, Mayberg HS. Stuck in a rut: rethinking depression and its treatment. Trends Neurosci. 2011; 34:1–9. [PubMed: 21067824]

Hutchison RM, Womelsdorf T, Allen EA, Bandettini PA, Calhoun VD, Corbetta M, Della Penna S, Duyn JH, Glover GH, Gonzalez-Castillo J, Handwerker DA, Keilholz S, Kiviniemi V, Leopold DA, de Pasquale F, Sporns O, Walter M, Chang C. Dynamic functional connectivity: promise, issues, and interpretations. Neuroimage. 2013a; 80:360–378. [PubMed: 23707587]

Hutchison RM, Womelsdorf T, Gati JS, Everling S, Menon RS. Resting-state networks show dynamic functional connectivity in awake humans and anesthetized macaques. Hum Brain Mapp. 2013b; 34:2154–2177. [PubMed: 22438275]

Jones DT, Vemuri P, Murphy MC, Gunter JL, Senjem ML, Machulda MM, Przybelski SA, Gregg BE, Kantarci K, Knopman DS, Boeve BF, Petersen RC, Jack CR Jr. Non-stationarity in the “resting brain's” modular architecture. PLoS One. 2012; 7:e39731. [PubMed: 22761880]

Keilholz SD, Magnuson ME, Pan WJ, Willis M, Thompson GJ. Dynamic properties of functional connectivity in the rodent. Brain Connect. 2013; 3:31–40. [PubMed: 23106103]

Liang, Z.; Liu, X.; Zhang, N. Dynamic resting-state functional connectivity in awake animals. International Society for Magnetic Resonance in Medicine; Italy: May. 2014

Liu X, Chang C, Duyn JH. Decomposition of spontaneous brain activity into distinct fMRI co-activation patterns. Front Syst Neurosci. 2013; 7:101. [PubMed: 24550788]

Liu X, Duyn JH. Time-varying functional network information extracted from brief instances of spontaneous brain activity. Proc Natl Acad Sci U S A. 2013; 110:4392–4397. [PubMed: 23440216]

Liu, X.; Yanagawa, T.; Leopold, DA.; Fujii, N.; Duyn, JH. Electrophysiological correlate of fMRI resting-state networks in macaques. International Society for Magnetic Resonance in Medicine; Italy: May. 2014

Majeed W, Magnuson M, Hasenkamp W, Schwarb H, Schumacher EH, Barsalou L, Keilholz SD. Spatiotemporal dynamics of low frequency BOLD fluctuations in rats and humans. Neuroimage. 2011; 54:1140–1150. [PubMed: 20728554]

Petridou N, Gaudes CC, Dryden IL, Francis ST, Gowland PA. Periods of rest in fMRI contain individual spontaneous events which are related to slowly fluctuating spontaneous activity. Hum Brain Mapp. 2013; 34:1319–1329. [PubMed: 22331588]

Rousseeuw PJ. Silhouettes: a graphical aid to the interpretation and validation of cluster analysis. Journal of computational and applied mathematics. 1987; 20:13.

Rubinov M, Sporns O. Weight-conserving characterization of complex functional brain networks. Neuroimage. 2011; 56:2068–2079. [PubMed: 21459148]

Sakoglu U, Pearlson GD, Kiehl KA, Wang YM, Michael AM, Calhoun VD. A method for evaluating dynamic functional network connectivity and task-modulation: application to schizophrenia. MAGMA. 2010; 23:351–366. [PubMed: 20162320]

Shirer WR, Ryali S, Rykhlevskaia E, Menon V, Greicius MD. Decoding subject-driven cognitive states with whole-brain connectivity patterns. Cereb Cortex. 2012; 22:158–165. [PubMed: 21616982]

Smith SM, Miller KL, Moeller S, Xu J, Auerbach EJ, Woolrich MW, Beckmann CF, Jenkinson M, Andersson J, Glasser MF, Van Essen DC, Feinberg DA, Yacoub ES, Ugurbil K. Temporally-independent functional modes of spontaneous brain activity. Proc Natl Acad Sci U S A. 2012; 109:3131–3136. [PubMed: 22323591]

Tagliazucchi E, Balenzuela P, Fraiman D, Chialvo DR. Criticality in large-scale brain FMRI dynamics unveiled by a novel point process analysis. Front Physiol. 2012; 3:15. [PubMed: 22347863]

Toro R, Fox PT, Paus T. Functional coactivation map of the human brain. Cereb Cortex. 2008; 18:2553–2559. [PubMed: 18296434]

van den Heuvel MP, Hulshoff Pol HE. Exploring the brain network: a review on resting-state fMRI functional connectivity. Eur Neuropsychopharmacol. 2010; 20:519–534. [PubMed: 20471808]

Wong CW, Olafsson V, Tal O, Liu TT. The amplitude of the resting-state fMRI global signal is related to EEG vigilance measures. Neuroimage. 2013; 83:8.

Highlights

- Utilize Co-Activation Patterns to develop detailed metrics of brain dynamics
- Compare brain dynamics during rest and sustained working memory with these metrics
- Demonstrate reduced brain dynamics during WM compared to rest

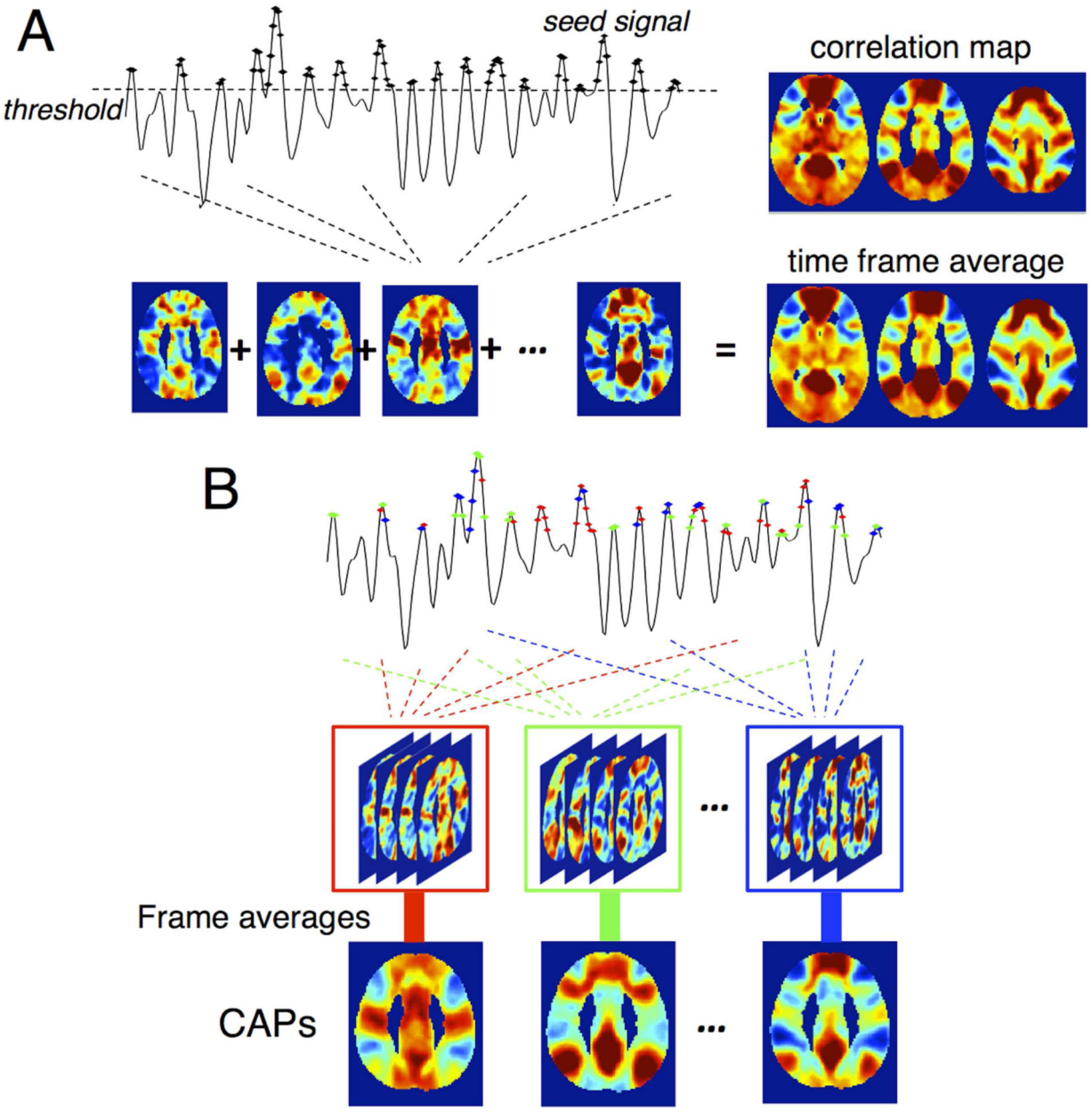

Fig. 1.

Illustration of CAP analysis in (Liu and Duyn, 2013) with the resting state datasets in this study (see section 2.2 Experiments and Analysis). (A) Conventional seed-based correlation map can be replicated by averaging time frames when the seed signal exhibits relatively large BOLD contrasts; (B) The scheme to generate CAPs. Different colors indicate different CAPs in temporal clustering.

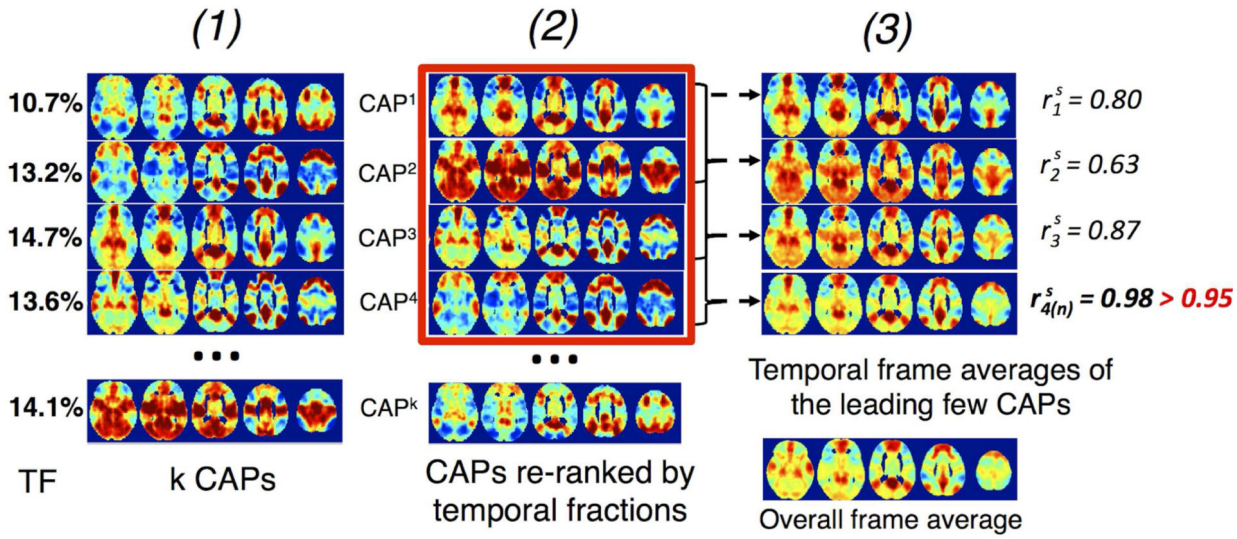

Fig. 2.

Steps to extract the dominant CAP-set for each cluster number *k*. (1) extract *k* CAPs, and their temporal occurrence fractions, '*TF*'; (2) reorder the *k* CAPs in descending *TF as CAP*^{1}, *CAP*^{2}, ... *CAP*^{k}; (3) compute $\{r_m^s\}_{1\leq m\leq k}$, spatial similarity of the weighted (by *TF*) average of the top-ranked CAPs with the overall frame average. Top-ranked CAPs $\{CAP^j\}1\leq j\leq n$ with $\{r_{n-1}^s < r_{thres}^s\}$ & $\left\{\prod_{p\geq n} \boldsymbol{I}\left\{r_p^s \geq r_{thres}^s\right\}\right\}$ (in red rectangle) comprise the dominant CAP-set at *k*.

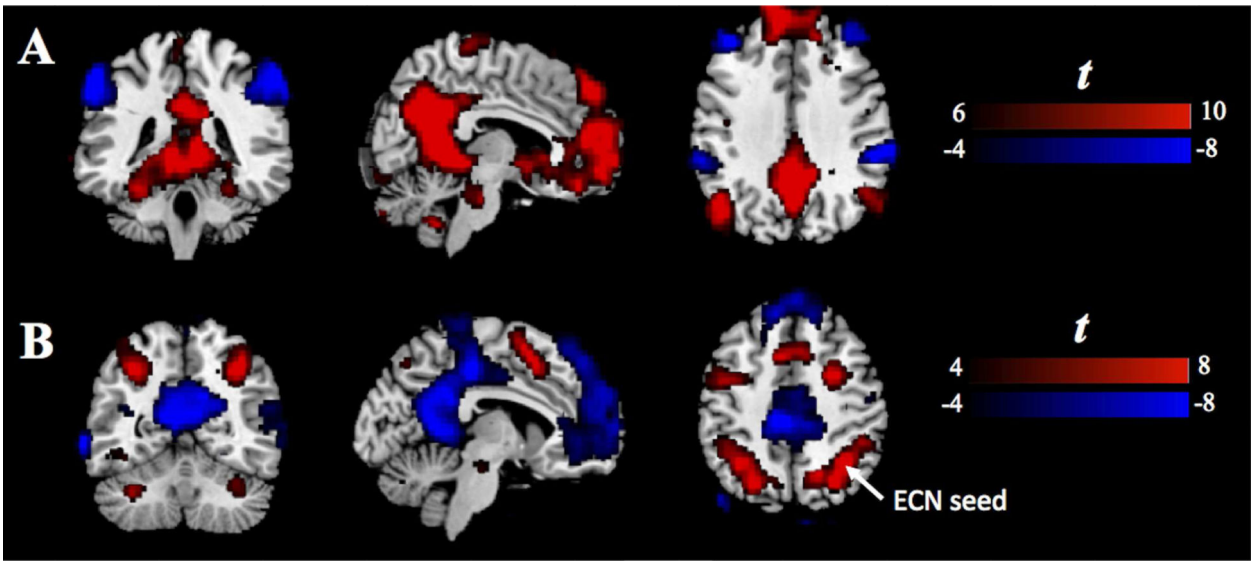

Fig. 3.

(A) The group t-test result of the positive and negative correlations with respect to the DMN-seed at rest. (B) The group t-test result of the activation in response to the 2-back WM task. ECN-seed is a local maximum, indicated by white arrow.

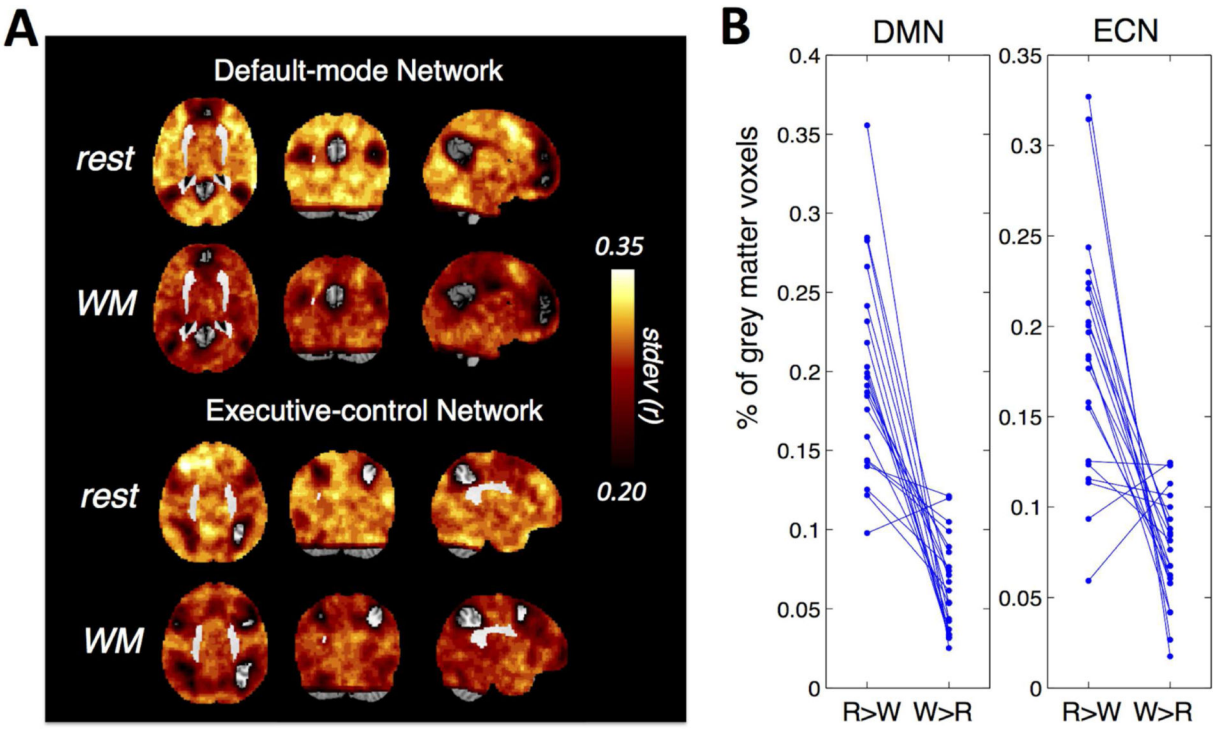

Fig. 4.

(A) Variability (standard deviations) over the sequence of 1-min sliding-window correlations between each brain voxel and the DMN and ECN seeds, averaged across 21 subjects; (B) Spatial extent of grey matter voxels with higher linear correlation variations during rest compared to WM task vs. the other way around for each subject (the difference of variability is thresholded at 0.1). 'R' stands for 'rest', 'W' stands for 'WM task'. Each blue straight line connects the percentage values ('R>W' and 'W>R') of a single subject.

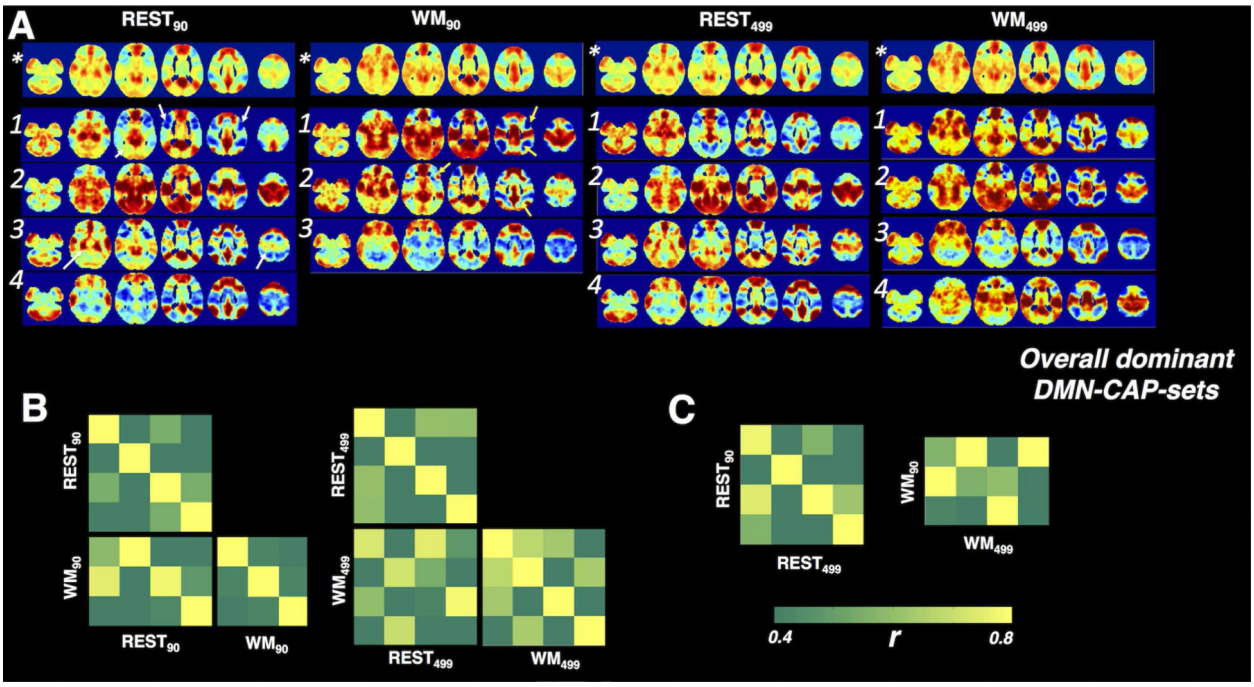

Fig. 5.

(A) The spatial profiles of the dominant CAP-sets associated with DMN. Numbers identify CAPs in each set, (*) denotes the overall frame average. (B) The spatial similarity covariance matrices between the overall dominant REST-CAP-set and WM-CAP-set for DMN, and within each dominant CAP-set. (C) The spatial similarity between the "overall dominant CAP-sets" derived with ROI_{90} and ROI_{499_W}.

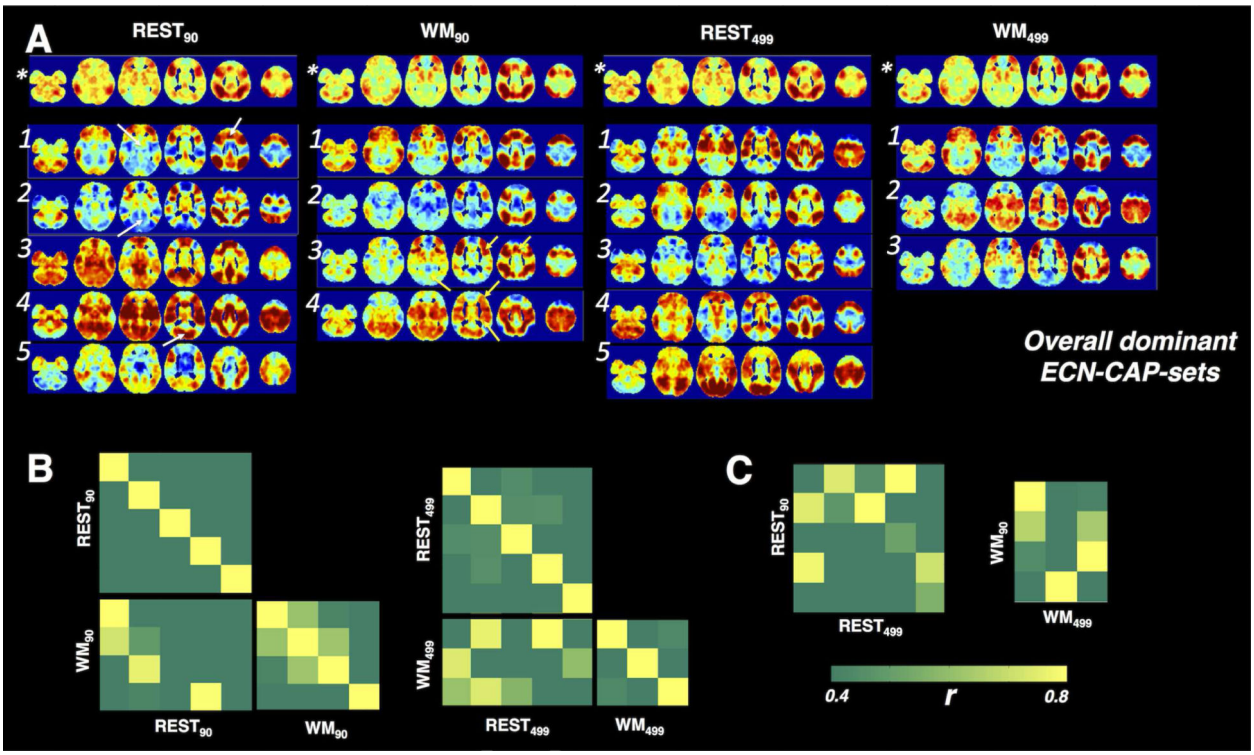

Fig. 6.

(A) The spatial profiles of the dominant CAP-sets associated with ECN. Numbers identify CAPs in each set, (*) denotes the overall frame average. (B) The spatial similarity covariance matrices between the overall dominant REST-CAP-set and WM-CAP-set for ECN, and within each dominant CAP-set. (C) The spatial similarity between the "overall dominant CAP-sets" derived with ROI_{90} and ROI_{499w}.

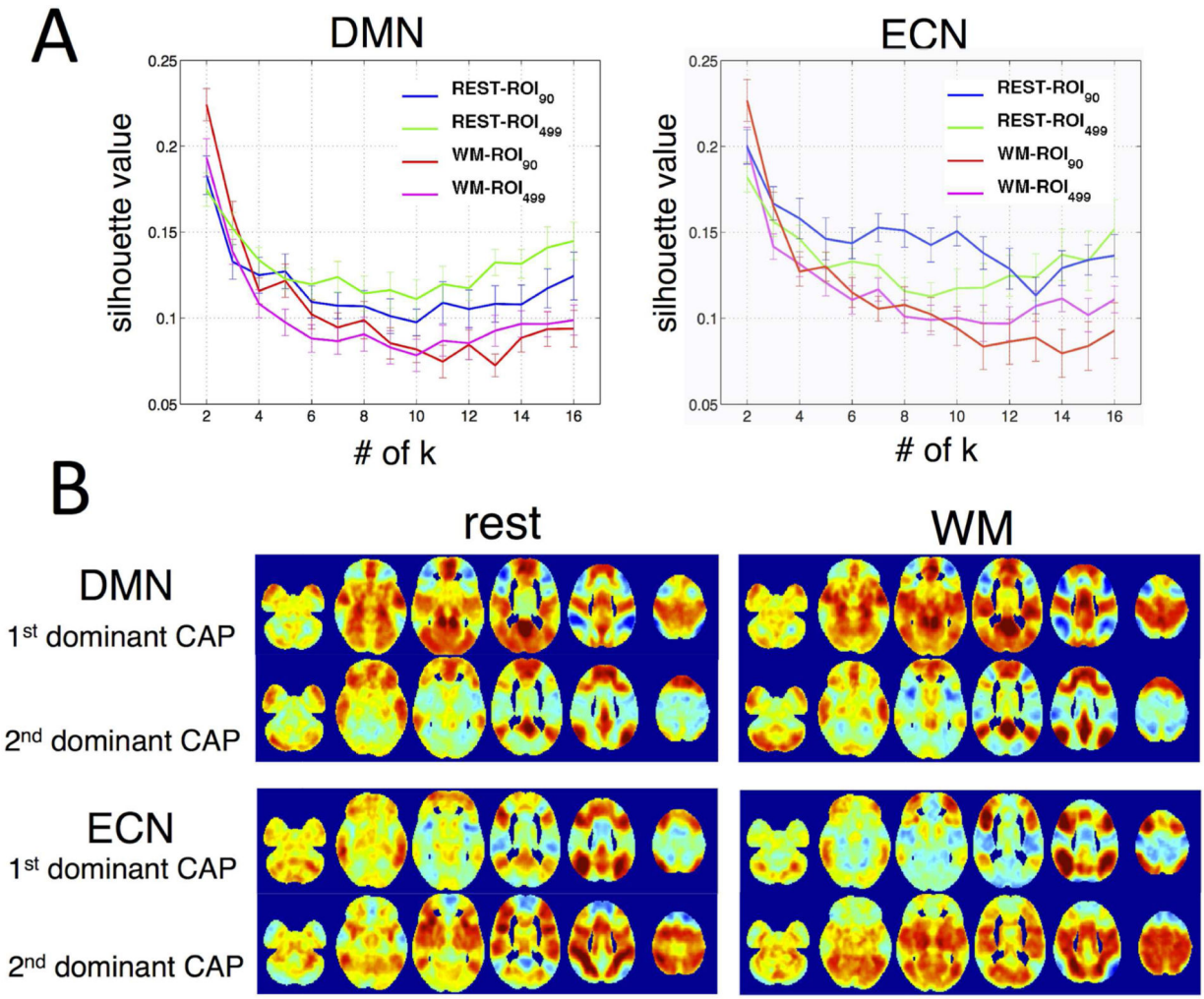

Fig. 7.

(A) Silhouette scores as a function of cluster numbers. Higher silhouette scores correspond to higher similarity between cluster members, i.e. more appropriate clustering. Results indicate $k = 2$ is best for both DMN and ECN. (B) The spatial patterns of the $1^{st}/2^{nd}$ dominant CAPs derived from ROI_{90}.

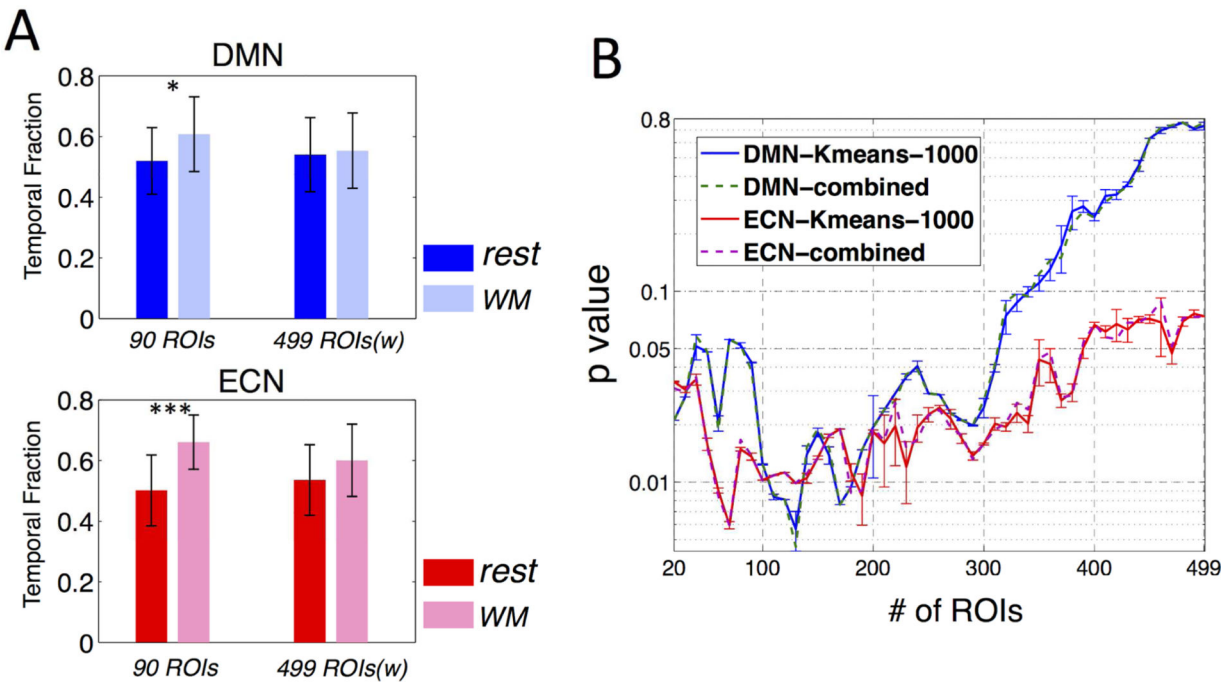

Fig. 8.

(A) Temporal fractions of the 1st dominant CAPs during sustained WM task compared to rest ($p<0.05$ *, $p<0.00005$ ***); (B) P values (group paired t-test, the temporal fraction of the 1st dominant CAP during WM task compared to rest) as a function of number of ROIs (in descending order of importance in differentiating two CAPs, see text 3.2.2 Temporal fractions of the 1st dominant CAP) included in the initial K-means clustering, where '-1000' indicates the mean and standard deviation of t values associated with the 1000 K-means clustering results, and 'combined' indicates the t value of the synthesized clustering result from the 1000 K-means trials (see text 2.2.7 CAP analysis).

Table 1

Summary of the correspondences between DMN-CAPs associated with different states (REST/WM task) and ROI sets (ROW_{90}/ROL_{499w}). See Fig. 5 for the spatial patterns of the corresponding CAPs.

DMN-CAPs			
$REST_{90}$ ↔ $REST_{499w}$	**WM_{90} ↔ WM_{499w}**	**$REST_{90}$ ↔ WM_{90}**	**$REST_{499w}$ ↔ WM_{499w}**
CAP1 ↔ CAP1 $^{(*)}$	CAP1 ↔ CAP2 $^{(**)}$	CAP1/3 ↔ CAP2 $^{(*)/(*)}$	CAP1/3 ↔ CAP1 $^{(*)/(*)}$
CAP2 ↔ CAP2 $^{(***)}$	CAP2 ↔ CAP1 $^{(***)}$	CAP2 ↔ CAP1 $^{(**)}$	CAP2 ↔ CAP2/4 $^{(*)}$
CAP3 ↔ CAP3 $^{(*)}$	CAP3 ↔ CAP3 $^{(***)}$	CAP4 ↔ CAP3 $^{(**)}$	CAP4 ↔ CAP3 $^{(**)}$
CAP4 ↔ CAP4 $^{(***)}$			

Spatial similarity

$^{(*)}r > 0.70$

$^{(**)}r > 0.80$

$^{(***)}r > 0.90$

Table 2

Summary of the correspondences between ECN-CAPs associated with different states (REST/WM task) and ROI sets (ROI_{90}/ROI_{499w}). See Fig. 6 for the spatial patterns of the corresponding CAPs.

ECN-CAPs			
$REST_{90}$ ↔ $REST_{499w}$	**WM_{90} ↔ WM_{499w}**	**$REST_{90}$ ↔ WM_{90}**	**$REST_{499w}$ ↔ WM_{499w}**
CAP1 ↔ CAP4 $^{(**)}$	CAP1 ↔ CAP1 $^{(***)}$	CAP1 ↔ CAP1 $^{(**)}$	CAP2/4 ↔ CAP1 $^{(**),(*)}$
CAP2 ↔ CAP3 $^{(**)}$	CAP3 ↔ CAP3 $^{(***)}$	CAP2 ↔ CAP3 $^{(*)}$	CAP2 ↔ CAP3 $^{(*)}$
CAP4 ↔ CAP1 $^{(**)}$	CAP4 ↔ CAP2 $^{(***)}$	CAP4 ↔ CAP4 $^{(*)}$	

Spatial similarity

$^{(*)}r > 0.70$

$^{(**)}r > 0.80$

$^{(***)}r > 0.90$

Table 3

Summary of *k* s (K-means clustering numbers, within 2 ~ 16) that yield the "overall dominant CAP-sets" (see Fig. 5A, 6A) associated with different brain states/networks.

Dominant CAPs	rest	WM task
PCC-ROI$_{90}$	6,7,8,9,11, (10,14)	5,6,8,9, (NA)
PCC-ROI$_{499w}$	5,6,7,9,13,14,15, (10)	7,8,9,10,11, (5,6)
ECN-ROI$_{90}$	5,6,8, (11,13)	5,6,7,9,10,11, (8,12,13,14)
ECN-ROI$_{499w}$	5,6,7, (11)	5,7,9, (8,12,13,15)

To alleviate the dependence of the results on the spatial similarity threshold 0.95 (see 2.2.7 CAP analysis), clustering numbers, of which the corresponding dominant CAP-set contains the "overall dominant CAP-set" as the leading subsets but with extended quantity of CAPs, are also listed (in the parenthesis, NA means 'not found'). Using the CAP results of PCC-ROI$_{90}$ at rest as an illustration (supplementary Fig. S6), k = 9 gives the identical CAP-set as the "overall dominant CAP-set", while k = 10 contains 5 CAPs, and the leading 4 CAPs are the same as the "overall dominant CAP-set".

Table 4

Summary of CAPs at k = 2. TF: temporal fractions of the 1st dominant CAP; AF: alternation frequencies between the 1st and 2nd dominant CAPs, expressed as number of switches. P values are calculated in paired-t tests.

Subject	PCC-ROI$_{90}$		PCC-ROI$_{499w}$		ECN-ROI$_{90}$		ECN-ROI$_{499w}$	
	TF(%) (rest/WM) p = 0.013	**AF (rest/WM) p = 0.13**	**TF(%) (rest/WM) p = 0.76**	**AF (rest/WM) p = 0.065**	**TF(%) (rest/WM) p=3.5e-5**	**AF (rest/WM) p = 0.52**	**TF(%) (rest/WM) p = 0.074**	**AF (rest/WM) p=0.88**
1	39/69	15/11	64/67	12/15	39/46	18/19	57/56	20/13
2	49/65	18/21	58/56	18/23	26/28	13/17	76/71	14/19
3	42/74	16/12	65/56	17/23	39/38	19/14	68/49	19/21
4	51/64	16/15	56/68	16/13	39/32	18/18	63/68	18/21
5	53/56	18/17	51/50	21/17	47/28	15/14	61/60	17/16
6	58/47	17/18	54/40	19/24	46/44	15/18	57/44	13/20
7	49/57	15/20	60/54	18/24	58/44	15/18	39/46	15/19
8	50/71	17/17	58/63	16/21	58/32	12/13	56/56	18/17
9	67/76	19/13	39/74	20/17	38/36	16/14	49/47	20/16
10	72/76	10/15	28/69	14/19	65/39	20/18	40/63	22/16
11	47/39	15/15	53/36	19/13	46/57	15/10	64/42	17/12
12	46/75	15/15	56/72	17/17	71/22	12/18	36/69	14/22
13	53/67	17/22	50/67	16/22	60/29	18/19	50/53	22/18
14	63/58	20/17	35/57	20/20	44/29	21/16	72/79	19/10
15	50/51	13/22	64/47	16/21	49/33	21/17	49/69	15/14
16	71/51	10/17	38/40	16/16	54/17	17/13	53/86	21/13
17	25/38	11/14	81/38	16/14	36/29	17/18	64/58	18/20
18	47/64	15/15	64/58	19/17	58/35	16/22	40/50	16/25
19	63/46	16/19	49/40	16/23	51/26	18/20	46/68	21/24
20	46/56	17/27	65/43	15/19	63/31	12/21	47/69	14/23
21	53/76	16/15	49/68	14/13	65/38	15/18	39/58	20/18

Table 5

Summary of changes of the dominant CAP-sets during WM task compared to rest. Results associated with both networks (DMN/ECN) and both ROI sets (ROI_{90}/ROI_{499w}) demonstrated more consistent network patterns in the format of either ‘reduced number of dominant CAPs’ or ‘increased spatial similarity’ across different CAPs.

	Changes of the dominant CAP-sets	
	Reduced # of CAPs	**Increased spatial similarity**
DMN-ROI_{90}	yes	
DMN-ROI_{499w}		yes
ECN-ROI_{90}	yes	yes
ECN-ROI_{499w}	yes	